Molecular simulation of subcritical crack growth under dry conditions in a model brittle glass

Binghui Deng, Swastik Basu, Liping Huang, Yunfeng Shi*

Department of Materials Science and Engineering, Rensselaer Polytechnic Institute, Troy, NY

*Corresponding author: Yunfeng Shi, shiy2@rpi.edu

Abstract

Subcritical crack growth can occur under a constant applied load below the threshold value for catastrophic failure, also known as static fatigue. Here we report how a crack grows under a combination of stress intensity factor (K) and temperature in a model brittle glass using molecular dynamics simulations. The model glass is under dry conditions thus avoiding the complexity of corrosion chemistry. The crack growth rate is shown to be inconsistent with the commonly used subcritical crack growth model rooted in the transition state theory (TST), in which the applied stress intensity factor reduces the transition barrier. A new subcritical crack growth model is proposed with a constant barrier and a K-dependent prefactor in TST, representing the size of the region for potential bond breaking. The thermomechanical condition for subcritical crack growth is also mapped in the K-T domain, in between elastic deformation and catastrophic fracture regimes. Finally, we show substantial crack self-healing once the applied load is removed, under the thermodynamic driving force of surface energy reduction. Our findings provide new insights into the mechanochemical coupling during static fatigue and call for experimental investigation of whether the activation energy is K-dependent.

Keywords: molecular dynamics, subcritical crack growth, deformation map, transition state theory, static fatigue.

1. Introduction

Brittle solids such as window glass break abruptly without apparent plastic deformation, while ductile solids such as copper exhibit extensive plastic deformation before the ultimate failure. The fracture of brittle solids is highly sensitive to the presence of defects, leading to the concept of stress intensity factor (dependent on both external loading and defect size) as the proper mechanical stimuli for fracture. The conventional picture is that, as the applied stress-intensity factor increases monotonically, no crack growth is expected until the stress-intensity factor reaches a threshold value otherwise known as the fracture toughness. Contradicting to the above simplified narrative, crack growth is possible at least for some brittle solids even when the applied stress-intensity factor is below its fracture toughness, which is termed subcritical crack growth, or delayed fracture. The subcritical crack growth under a constant load is termed "static fatigue",[1] while crack growth under a varying load is termed "cyclic fatigue". Chemicals present in the environment can significantly affect the subcritical crack growth, involving complex interplay of diffusion, reaction and deformation, which is generally termed "stress-corrosion cracking". Subcritical crack growth is of primary importance affecting long-term reliability of glassy materials under stress. For instance, thermally or chemically tempered glasses with substantial internal stress distribution; nuclear waste glass [2] subjected to elevated temperature, high pressure and corrosive environment over a thousand to one million years of intended service duration; glass substrates need to withstand high temperature during processing [3] and elevated/cryogenic temperature during service.

There have been considerable research efforts both experimentally and theoretically to understand subcritical crack growth in glasses. Experimentally, both double-cantilever cleavage [4,5] and single pre-cracked beam method [6] can be used to achieve stable crack growth. Wiederhorn carried out double-cantilever cleavage experiments on six different glasses in vacuum, under various loads and temperatures.[4] Subcritical crack growth was observed in four glasses, but not in fused silica nor borosilicate glass. Both fused silica and borosilicate glass were classified by Wiederhorn to be "abnormal glasses", as Wiederhorn reasoned, due to "abnormal" thermal and mechanical properties. Wiederhorn extended the formulation of Charles and Hillig[7–10] on how crack growth rate is governed by thermomechanical stimuli. Similar theory has also been developed by Wan, Lathabai and Lawn.[11] The essence of these formulations roots in the transition state theory to describe chemical reaction, which is thermally activated with a barrier that is dependent on mechanical stimuli in terms of the stress intensity factor. The current subcritical crack growth theory relies heavily on continuum description of the stress distribution around ideal-shaped cracks. For instance, Wiederhorn's theory[4] considered a perfect elliptical crack which has a curvature of 0.5 nm, at which scale continuum mechanics formula is no longer valid due to the atomic discreteness. Recent experimental work on glass fiber bundle under static fatigue provides useful yet indirect crack growth information. [12] On the simulation side, there have been active development of phase-field modeling to describe fatigue crack growth by improving existing formulation to enable crack growth subcritically. [13,14] In addition, a new

kinetic model has been proposed combining existing crack growth model with viscoelastic relaxation leading to a thresholding behavior. [15] However, these modeling works provide limited insights into the thermomechanical origin of crack extension at the atomic level. There are a number of works on subcritical crack growth in wet conditions. Silva, et al, have employed multi-scale simulation with classical and semi-empirical molecular orbital methods to study effect of water in deformation of silica nanorod, in which they show the reaction barrier is reduced by the applied stress.[16] ReaxFF force field has been used to model the fracture of a nm-sized quartz crystal under stress with water.[17,18] Unfortunately, there appears to be very little atomic-level modeling work on dry subcritical crack growth in glasses. Rimsza, et al, reported crack growth in silica in both dry and wet conditions, yet under a varying applied stress intensity factor.[19] Probably due to the small system size without controlling the stress intensity factor, crack velocity as a function of stress intensity factor is not reported. It should be noted that experimental and computational investigations on dynamic crack propagation [20,21] generally focus on crack velocity regime that is on the order of the velocity of sound. Such crack growth cannot be considered as subcritical crack growth, even with apparently low velocities, without the knowledge of the instantaneous applied stress intensity factor.

Here, we report a systematic study on subcritical crack growth under dry conditions in a model glass using molecular dynamics (MD) simulations. Importantly, we utilized a new simulation protocol of constant stress intensity factor (constant-K) to control the loading of a pre-cracked sample in a microtension setup. Together with a thermostat, the crack growth rate can be reliably measured for a given combination of K and T. Our simulations show that subcritical crack growth under dry conditions is indeed thermally activated yet does not conform to the original Wiederhorn's theory. Consequently, an alternative crack growth rate formula was proposed which is also derived from the transition state theory. In addition, a simple classification of deformation modes based on crack extension was proposed: no crack extension (elastic deformation), stable and slow crack extension (subcritical crack growth), unstable crack extension (catastrophic failure). Such classification enables the creation of a deformation mechanism map in the domain of K and T. Lastly, upon unloading, self-healing was observed in samples undergoing subcritical crack growth.

2. Simulation methodology

2.1. Interatomic potential

Our MD simulations are carried out in LAMMPS [22] with customized force fields. In this work, we employed a modified binary Lennard-Jones (LJ) potential ϕ_{mLJ}, which is based on Wahnstrom's binary LJ potential [23] with a shorter cutoff to include only the first nearest neighbors. The additional energy penalty term is motivated by Dzugutov potential, somewhat mimicking the Friedel's oscillations.[24–27] We have demonstrated that, by controlling this energy penalty term, the intrinsic ductility of model glass can be tuned from ductile to brittle.[28–32] The

alloy consists of two equimolar species, which will be referred to as *S* and *L* for small and large atoms. For completeness, the formulation and parameterization are as follows. The species dependent pair-wise interaction (α, β represents species) consists of a conventional LJ form ϕ_{LJ} shifted and truncated at a pair-dependent cutoff $r_{c,\alpha\beta}$, with an additional energy penalty term ϕ_{Bump} effective only between $r_{s,\alpha\beta}$ and $r_{e,\alpha\beta}$.

$$\phi_{mLJ}(r) = \phi_{LJ}(r) + \phi_{Bump}(r) \tag{1}$$

$$\phi_{LJ}(r) = \begin{cases} 4\varepsilon_{\alpha\beta}\left(\frac{\sigma_{\alpha\beta}^{12}}{r^{12}} - \frac{\sigma_{\alpha\beta}^{6}}{r^{6}}\right) - 4\varepsilon_{\alpha\beta}\left(\frac{\sigma_{\alpha\beta}^{12}}{r_{c,\alpha\beta}^{12}} - \frac{\sigma_{\alpha\beta}^{6}}{r_{c,\alpha\beta}^{6}}\right), & r < r_{c,\alpha\beta} \\ 0, & r \geq r_{c,\alpha\beta} \end{cases} \tag{2}$$

$$\phi_{Bump}(r) = \begin{cases} 0, & \mathrm{r} < r_{s,\alpha\beta} \\ \varepsilon_B\varepsilon_{LL} \cdot sin^2\left(\pi\frac{r_{c,\alpha\beta}-r}{r_{c,\alpha\beta}-r_{s,\alpha\beta}}\right), & r_{e,\alpha\beta} > r \geq r_{s,\alpha\beta} \\ 0, & \mathrm{r} \geq r_{e,\alpha\beta} \end{cases} \tag{3}$$

The potential parameters are listed in Table 1, normalized by internal units of ε_0, σ_0 and m_0 for energy, length and mass, respectively. The reference time scale is $t_0 = \sigma_0\sqrt{\frac{m_0}{\varepsilon_0}}$. The two types of atoms have different masses: $m_L = 2m_0, m_s = m_0$. All physical quantities will therefore be expressed in SI units following the conversion in a previous report [28]: $\sigma_0 \approx 2.7$ Å; $m_0 \approx 46$ amu; $\varepsilon_0 \approx 0.151$ eV; $t_0 \approx 0.5$ ps. A standard velocity Verlet integrator was used with a timestep of 2.5 fs.

Table 1: List of potential parameters.

Pair	$\varepsilon_{\alpha\beta}/\varepsilon_0$	$\sigma_{\alpha\beta}/\sigma_0$	$r_{\alpha\beta,s}/\sigma_0$	$r_{\alpha\beta,e}/r_{\alpha\beta,c}$	ε_B	$r_{\alpha\beta,c}/\sigma_0$
L-L	1.0	1.0	1.2	1.0	1.1	1.40000
L-S	1.0	0.91667	1.1	1.0	1.1	1.28333
S-S	1.0	0.83333	1.0	1.0	1.1	1.16667

2.2. Sample preparation

The glassy samples were prepared by quenching a well-equilibrated liquid at 2105 K to 28 K isochorically for a total cooling time of 2500 ps, consistent with prior studies.[29] Generally higher cooling rate leads to more disordered local structure and less brittle glass.[28] The glass transition for the model glass is around 800 K. The glass transition temperature was estimated as the temperature corresponding to the peak of the specific heat at constant volume during cooling, at which the system loses a considerable number of degrees of freedom. The average atomic volume of the system during cooling in an NVT ensemble is a constant at 0.0173 nm^3, which was chosen to reach a near-zero final pressure for the final glassy sample. It should be noted that there was a compressive pressure during cooling. The periodic boundary conditions (PBCs) were applied in

three-dimensions during the cooling process. Any minute residual stress from cooling will be relaxed using an NPT ensemble such that the final glassy sample is stress-free. Temperature control and stress control during the MD simulations follow the standard Nose-Hoover formulation.[33,34] The density of the glassy sample is 6.59 g/cc. Its average atomic volume is about 0.0174 nm^3.

For conventional uniaxial tension test, we prepared a glassy sample using the above procedure with a geometry of 5.2 nm by 5.2 nm by 15.5 nm, consisting of 24000 atoms. The sample was first subjected to uniaxial tension test. As shown in Figure 1, the glassy sample deforms elastically then fails brittlely at about 14% of strain. From the uniaxial tension test, the Young's modulus was measured to be about 95 GPa, and the Poisson's ratio was measured to be about 0.26. The longitudinal wave speed is about 4.2 km/s.

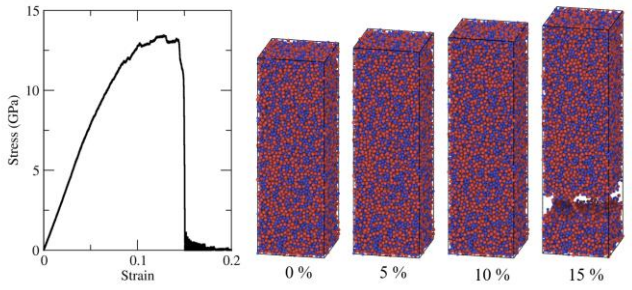

Figure 1. Uniaxial tension test of a glassy sample showing brittle fracture with its stress-strain curve (left) and deformation morphologies at four different strains (right). Red and blue denote L and S particles, respectively.

For microtension test to investigate subcritical crack growth, we prepared a glassy sample with a pre-crack as shown in Figure 2A. We first prepared a glassy sample with a geometry of 15.6 nm by 15.5 nm by 2.6 nm with the same cooling procedure containing 36000 atoms, then replicated the sample 6 times in both X and Y direction to obtain a final sample of 94 nm by 93 nm by 2.6 nm. As the stress field due to the pre-crack is highly inhomogeneous, there is no artificial periodicity in deformation morphology arising from the replication. The z-direction was intentionally set to be very thin to extend the sample in X and Y direction while maintaining a manageable system size. The pre-crack was created by removing any atom within a through-the-thickness diamond-shaped region in the center of the sample, with a height of 4.0 nm and a length of 18.9 nm. The diamond-shaped pre-crack was also used in our earlier work.[28,31]

2.3. Constant-*K* microtension test

The glassy sample as shown in Figure 2A is subjected to tension in the Y direction, while maintaining zero stress in the X direction. The thickness was kept constant mimicking the plane strain condition. Periodic boundary conditions were applied in all three directions. It has been well established that continuum elastic description is highly consistent with MD simulation results for amorphous systems, even better than crystalline systems.[35] We have also carefully examined the critical stress-intensity factor K_{IC} (as well as critical *J*-integral for fracture J_{IC}) measured from MD is a material property, independent of the pre-crack size.[31] Figure 2B shows the local normal stress distributions (σ_{yy}) at different loadings agree well the Westergaard's solution,

$$\sigma_{yy} = \sigma_{farfield} / \sqrt{1 - \left(\frac{c}{x}\right)^2} \quad (4)$$

$\sigma_{farfield}$ is the far-field stress (measured in MD simulations over a horizontal slice farthest away from the crack with a height of 2.2 nm and throughout the thickness). x is the distance away from the crack center. c is the half crack size. To identify the crack tips, we calculated the local density averaged over a grid size of 0.5 nm by 0.68 nm by 2.6 nm. Going from left to right, the left crack tip is where the local density decreases to about 70% of the bulk value, while the right crack tip is where the local density increases to about 70% of the bulk value. The crack tip is allowed to deviate vertically (Y direction) from the original pre-crack by up to 3 nm, as the crack growth is not ideally horizontal. Figure 2B shows that, for our glassy sample with the pre-crack, continuum fracture mechanics are valid, and the stress-intensity factor K_I is the appropriate representation of the

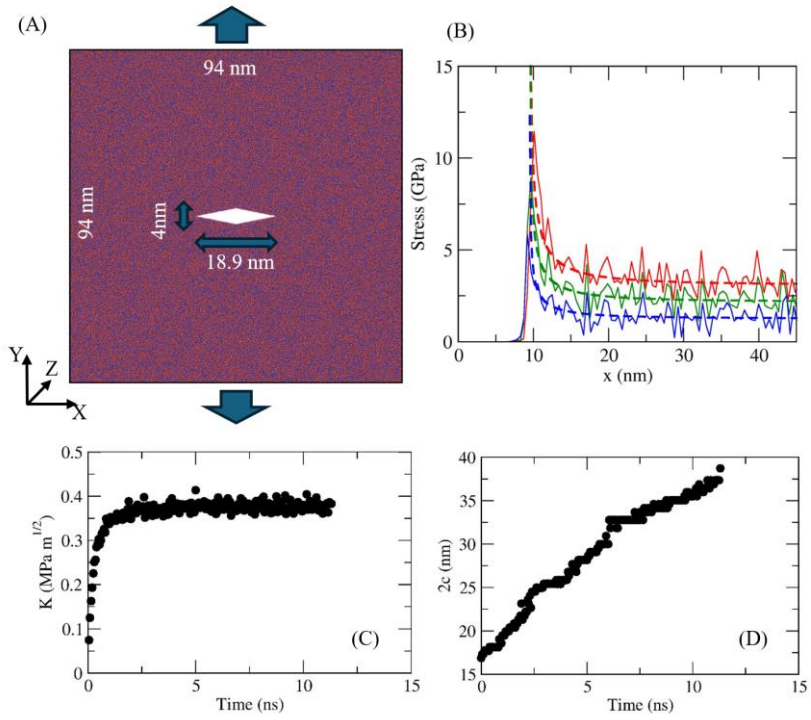

Figure 2. (A) Glassy sample geometry for microtension test. (B) Local normal stress (σ_{yy}) distribution along the center of the sample (averaged over 1.35 nm in Y direction and the entire thickness) as a function of distance away from the center of the crack for K_I=0.22, 0.38 and 0.54 MPa$\cdot\sqrt{m}$, colored as blue, green and red. The dashed lines are Westergaard's solutions with $\sigma_{farfield}$ measured as 1.2, 2.2, and 3.1 GPa. The temperature was kept at 52 K to suppress crack growth. (C) Applied stress-intensity factor K_I stabilizes at the target value of 0.38 MPa$\cdot\sqrt{m}$. (D) The crack size increases over time under a constant K_I. The temperature was kept at 210 K for MD simulation in panes (C, D).

mechanical stimuli for the microtension test. K_I is calculated as follows, with the Feddersen analytical form [36] of finite width correction (almost identical to Isida's correction factor from numerical calculation [37], with higher accuracy [38] than Irwin's correction [39,40]):

$$K_I = \sigma_{farfield} \sqrt{\pi c} \left(sec\left(\frac{\pi c}{W}\right)\right)^{\frac{1}{2}} \quad (5)$$

W is the sample width along X direction. If the instantaneous K_I is lower than the target value, a tensile strain rate proportional to the difference was applied, and vice versa. For instance, the initial tensile strain rate for a target K_I of 0.38 $MPa\cdot\sqrt{m}$ is 1.9E-4 ps^{-1}. In this way, a constant K_I microtension test can be achieved as shown in Figure 2C. A stable crack growth under the target K_I is shown in Figure 2D. Note that, although the nominal crack length is 18.9 nm (i.e., the length of the diamond-shaped pre-crack), the actual measured crack is slightly shorter (~16.8 nm) due to atomic rearrangement near the tip in response to the creation of the pre-crack. Together with a thermostat controlling the temperature, the crack growth rate can be measured for a given thermomechanical condition.

3. Results

3.1. Subcritical crack growth rate

Utilizing the constant-K microtension test, we systematically measured the subcritical crack growth rate over a range of stress intensity factors and a range of temperatures. The crack velocity can be obtained as the slope of crack length (up to 32.4 nm) over time (up to 25 ns) once the stress intensity factor stabilizes. In addition, five independent glass samples were used to obtain an

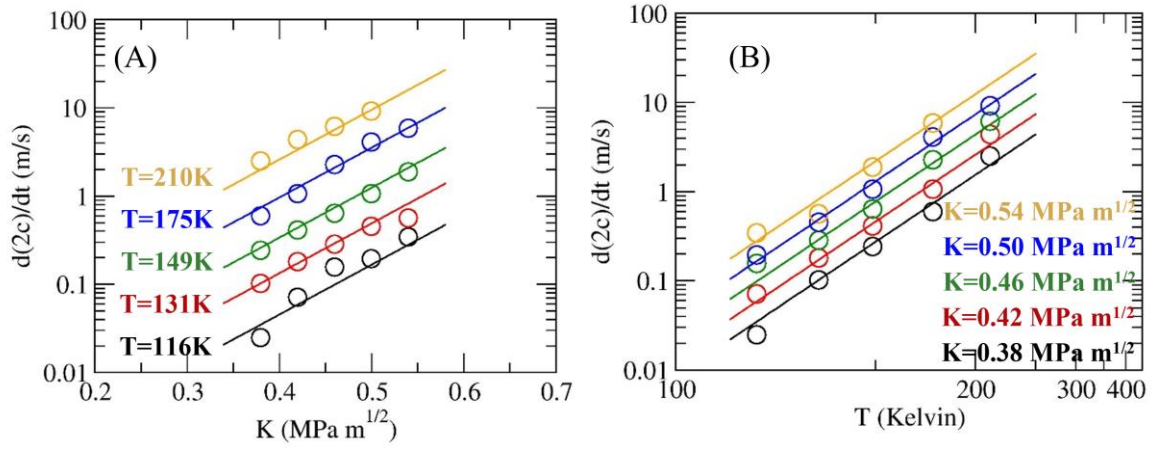

Figure 3. (A) Subcritical crack growth velocity appears to be exponentially dependent on the applied stress intensity factor. (B) Subcritical crack growth appears to be thermally activated in an Arrhenius plot, with a constant activation energy independent of the stress intensity factor. Solid lines are best fitting lines according to Eq. (7).

averaged crack growth rate to reduce fluctuation in crack growth probably due to structural heterogeneity.

To facilitate the discussion, the crack extension velocity (v) according to the existing subcritical crack growth theory, developed by Wiederhorn, Charles, Hillig, Lawn, and others [1,4,7–10,41–43] can be written as,

$$v = v_0 e^{-\frac{\Delta H^{\ddagger} - K_I b}{RT}} \quad (6)$$

Here, v_0, $\Delta H^{\ddagger}$, K_I, R, T is a velocity constant, activation enthalpy, stress intensity factor, gas constant, and temperature, respectively. b is a material conjugate variable to the stress intensity factor, assumed to be a constant.

Figure 3A shows the crack growth rate as a function of K_I at different temperatures, which is quite similar to experimental results by Wiederhorn on "normal" oxide glass under dry conditions. That is, the crack growth rate depends on K_I exponentially. It should be noted that, the slope in Figure 3A $dln(v)/dK_I$ appears to be a constant ($v=d(2c)/dt$ is the crack growth rate). This is in disagreement with Wiederhorn's subcritical crack growth model in which the slope is inversely proportional to the temperature ($-b/RT$, according to Eq. 6). In fact, a closer examination of Wiederhorn's data on aluminosilicate (Figure 2D in [4]), the slope of $dln(v)/dK_I$ seems also to be a constant. Moreover, the fitting by Wiederhorn for the highest two temperatures are noticeably worse than the other three temperatures.

To further examine Wiederhorn's model, the same crack growth data was presented in an Arrhenius plot under various K_I, which is shown in Figure 3B. It is clear that the activation energy is a constant regardless of the applied stress intensity factor. In other words, the stress intensity factor does not lower the reaction barrier, as assumed by Wiederhorn.[4] Instead, it appears that the stress intensity factor controls the prefactor of the overall crack growth (i.e. vertical shift in the Arrhenius plot as shown in Figure 3B), not coupled to the temperature. The common "mechanical assisted chemical reaction" picture, works well for high temperature creep,[44,45] yet seems to be not applicable for subcritical crack growth. It should be noted that the stress field in subcritical crack growth is highly inhomogeneous, while the stress field in high temperature creep is homogeneous. That is, K_I controls the size of the region for potential bond rupture and crack growth, not the actual amount of bond extension. Based on Figure 3, we propose the following crack growth model rooted also in transition state theory, yet with a constant reaction barrier. In this model, the effect of mechanical stimuli controls only the pre-factor of the chemical reaction. The crack growth rate is assumed to be proportional to chemical reaction rate,

$$v = v_0 \exp\left(\frac{K_I}{K_0}\right) \exp\left(-\frac{\Delta H^{\ddagger}}{RT}\right) \quad (7)$$

Here, v_0, $\Delta H^{\ddagger}$, K_I, R, T is a velocity constant, activation enthalpy, stress intensity factor, gas constant, and temperature, respectively. K_0 here serves as a reference stress intensity factor. Here, the activation enthalpy should be comprehended as the averaged activation energy over a bond stretching distribution at the pre-crack region. The solid lines in Figure 3 are from the new crack growth model, which agree with our MD simulation results. The best fit value for v_0, $\Delta H^{\ddagger}$, K_I are 2.0 m/s, 0.090 eV, and 0.076 $MPa\cdot\sqrt{m}$, respectively. It should also be noted that, Eq. (6) is equivalent to Eq. (7) under the condition that the parameter b is proportional to temperature.

3.2. Deformation mechanism map

As Wiederhorn discovered earlier,[4] brittle solids may either exhibit subcritical crack growth, or exhibit sudden failure without subcritical crack growth. Therefore, it is useful to understand, for the current model glass, the thermomechanical conditions on which subcritical crack growth mode is allowed. A total of 122 combinations of temperature and stress intensity factor were investigated using one glassy sample. The simulation time is up to about 4 ns. A simple deformation classification is described as follows, with examples shown in Figure 4A. If the crack grows from the initial 16.8 nm without load to less than 18.2 nm at the end of the simulation, the deformation mode is classified as elastic (blue diamonds in Figure 4A). The 1.4 nm crack extension can be considered as the atomic rearrangement of the crack tip upon tensile loading. If the crack grows uncontrollably across the entire sample within 4 ns, the deformation mode is classified as fracture (red triangles in Figure 4A). The stress intensity factor for sample undergoing fracture never reaches the intended target value in our constant-K simulations. For steady crack growth beyond 1.4 nm over 4 ns, the deformation mode is classified as subcritical crack growth (green disks in Figure 4A). As only one glassy sample was used to generate the deformation mechanism map, it is useful to examine sample-to-sample variation from our existing data of five independent samples discussed in Section 3.2. The other four independent samples agree with Figure 4B for all of the temperature and stress intensity factor combinations with one exception. For temperature of 116 K and stress intensity factor of 0.38 $MPa\cdot\sqrt{m}$ (very close to the boundary), two samples are classified as elastic agreeing with Figure 4B, while the other two are classified as subcritical crack growth.

As shown in Figure 4B, the deformation mechanism of the brittle solid with a pre-crack sensitively depends on both the stress-intensity factor and the temperature. At a given temperature, as the applied stress-intensity factor increases, the solid exhibits elastic deformation, subcritical crack growth and then fracture. Therefore, the boundary between the elastic regime and subcritical crack growth regime is the fatigue limit (dotted line in Figure 4B), while the boundary between the subcritical crack growth regime and the fracture regime is the fracture toughness (dashed line in Figure 4B). The fatigue limit seems to decrease as temperature increases, consistent with thermally activated bond rupture picture. The fracture toughness appears to increase first with temperature, which is probably due to toughening (for instance, local shear is promoted by the elevated temperature). At even higher temperatures, the subcritical crack growth rate is already

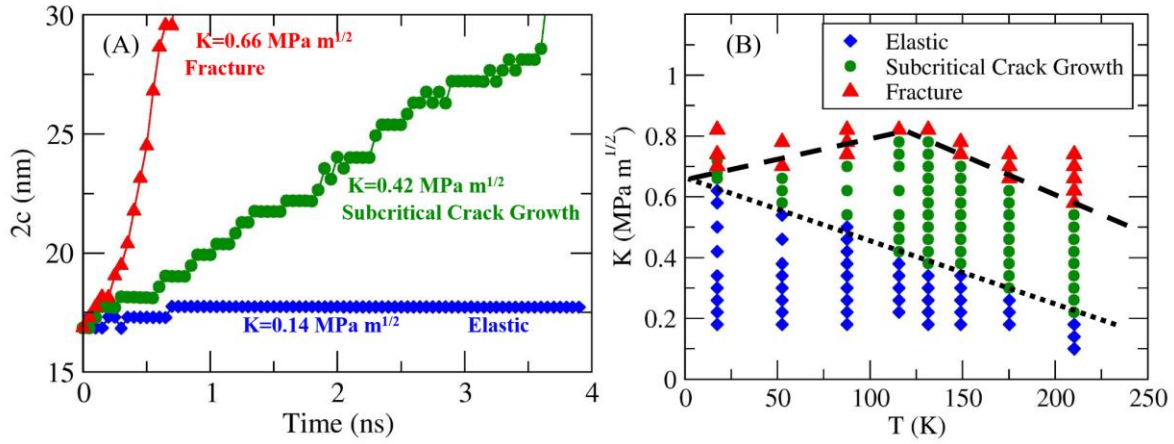

Figure 4. (A) MD simulations showing the crack growth behavior under three different stress intensity factors at a temperature of 210 K, showing elastic, subcritical crack growth and catastrophic facture behaviors. (B) Deformation mechanism map on K-T domain showing the subcritical crack growth regime. The boundary separates the elastic regime and the subcritical crack growth regime is essentially the fatigue limit (dotted line), while the boundary separates the subcritical crack growth regime and the fracture regime is the fracture toughness dashed line).

high enough to be classified as fracture, at which the fracture toughness reduces as the temperature increases.

It should be noted that both the fatigue limit and the fracture toughness are identified using criteria convenient to use for our MD simulations, which are consequently biased. For instance, our fatigue limit is likely to be overestimated, as MD simulation cannot detect very low crack velocity. Nonetheless, this deformation mechanism map shows that brittle solids can exhibit subcritical crack growth over large thermomechanical regime. More importantly, the range of stress intensity factor to induce subcritical crack growth seems to be very sensitive to the temperature. At the limiting case of zero Kelvin, there is no subcritical crack growth due to the absence of thermal agitation. These results suggest that the classification of glasses, based on whether they exhibit subcritical crack growth, need to take temperature into consideration.

3.3. Self-healing

Self-healing in oxide glasses have been observed by Wiederhorn [46] and Tomozawa.[5] Generally speaking, due to the driving force of minimizing surface energy, crack propagation can be reversed upon the removal of the applied load. Here, we first subjected a glassy sample with a K=0.54 MPa$\cdot\sqrt{m}$ of stress intensity factor for about 22 ns at 131 Kelvin, during which the crack extends from 16.8 nm to about 28.0 nm in length. Subsequently, this sample with 28 nm crack was then tested with different amounts of unloading to observe how the crack will evolve. Figure 5 shows the crack length as a function of time under various stress intensity factors including a

compressive stress intensity factor. The crack seems to maintain its length at 28 nm for K=0.46 and 0.30 MPa· $\sqrt{m}$, and fluctuate towards healing for K=0.14 MPa· $\sqrt{m}$. Only under K=0.0 and -0.14 MPa· $\sqrt{m}$, the crack heals substantially. The crack healing process also resembles the crack growth process, both of which are constituted by stochastic discrete bond formation or bond breaking events. It is likely that the crack healing kinetics is also governed by a rate equation based on transition state theory. It is important to note that, the healing is not ideal as there are a number of atomic-level voids present along the original crack path as shown in Fig. 5. This is not surprising given the temperature for self-healing is very low, and over a very short amount of time.

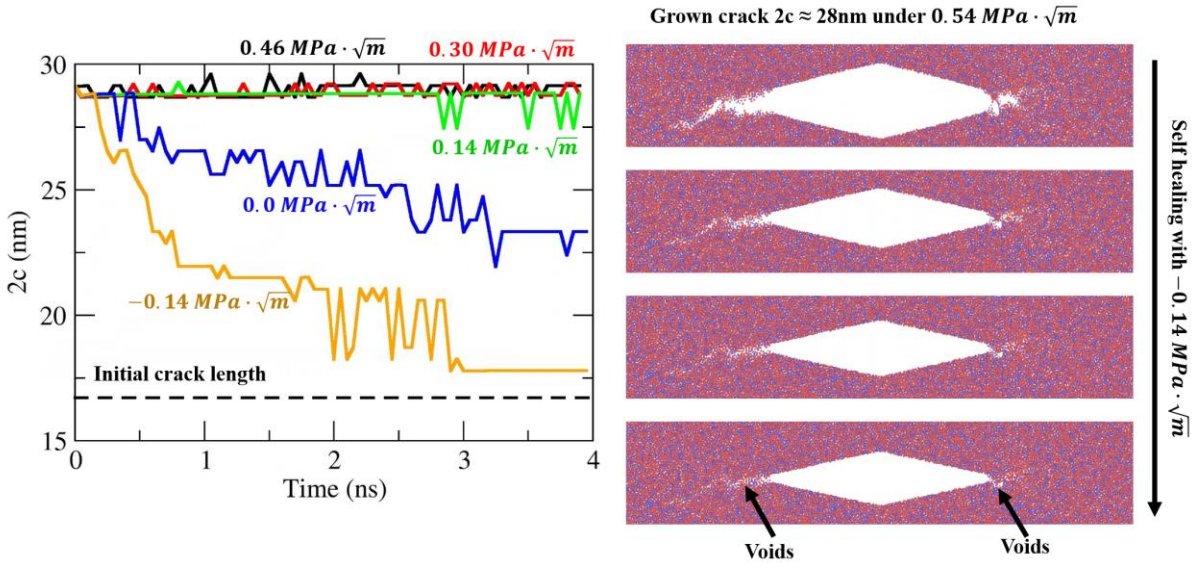

Figure 5. Self-healing of a crack that has grown subcritically under K=0.54 MPa· $\sqrt{m}$ and T=131 Kelvin for 22 ns from 16.8 nm to about 28.0 nm. Left pane shows the crack closing under different stress intensity factors from 0.46 to -0.14 MPa· $\sqrt{m}$. Right pane shows the crack closing morphology under -0.14 MPa· $\sqrt{m}$. Atomic-level voids can be seen along the healed crack.

4. Discussions

The model glass we used in this investigation is generally considered to be a model metallic glass. However, to our best knowledge, there is no experimental report of static fatigue in metallic glasses. This is likely due to the fact that typical metallic glasses are ductile locally (as opposed to brittle globally for instance under uniaxial tensile test) such that persistent crack growth cannot occur with a constant load subcritically. Our model glass was tuned to be extremely brittle by increasing the bump height ε_B to reduce local plasticity near the crack tip such that the crack can grow subcritically. A higher bump height leads to additional energy penalty of bond swapping, thus prohibiting plastic flow, which is also sensitively reflected by the Poisson's ratio.[28] The

current model glass with ε_B of 1.1 has a Poisson's ratio of 0.26 (much lower than typical metallic glasses ~0.3 or higher [29]). We have also tested a model glass with ε_B of 0.2, with a Poisson's ratio of 0.28, which exhibits no subcritical crack growth. Although the subcritical crack growth experiments were conducted typically on oxide glasses, the fundamental physical process of mechanically assisted chemical reaction also presents in our model glass. Therefore, the our subcritical crack growth formula can in principle be applied to oxide glasses. Our results call for experimental measurement of the activation energy as a function of stress intensity factor for oxide glasses to examine different formulations of subcritical crack growth. In addition, we plan to investigate subcritical crack growth in model oxide glasses in the near future.

The lowest crack growth rate measured here is close to 0.01 m/s (the MD simulation takes roughly two weeks), which is roughly two or more orders of magnitude higher than the highest subcritical crack growth rate measured in experiments. This gap is common between MD simulations and experiments, primarily due to the limited time scale MD simulation can access. Various characterization techniques, already used to measure the speed for dynamic cracks,[21] could help narrow this gap. As there is no other known competing subcritical crack growth mechanism to be activated at lower stress intensity factor, we fully anticipate that the crack growth rates for our model glass will follow the same trend to much lower values.

Lastly, for our new subcritical crack growth formula Eq. (7), K_I controls the size of the region for potential bond rupture and crack growth. It should be noted that this region (where bond rupture occurs) may be related but likely not identical to the fracture process zone (commonly identified as where local yield occurs). The precise spatial extension of this region is difficult to identify as one must distinguish between bond ruptures that ultimately lead to crack growth and bond rupture that only result in bond swapping or local shear. Further quantitative analysis is needed to identify such zone, the atomic-level criterion to identify such zone, and the precise spatial extent as a function of different stress intensity factors, so as to understand the exponential dependency according to Eq. (7).

5. Conclusions

We have systematically investigated the crack behavior of a model glass with a pre-existing crack under dry conditions, as a function of temperature and applied stress intensity factor using molecular dynamics simulations. A deformation mechanism map was given delineating elastic, subcritical crack growth and fracture regimes. Our model glass exhibits subcritical crack growth over a sufficiently wide thermomechanical regime, enabling the extraction of activation energy, which was found to be independent of the applied stress intensity factor. These findings suggest a new crack growth velocity formula, different from the commonly used Wiederhorn's model. Our results call for experimental measurement of the activation energy (via Arrhenius plot) as a function of stress intensity factor to ultimately judicate different formulations of subcritical crack growth.

Acknowledgements

We thank Professor Minoru Tomozawa and Professor Catalin Picu for fruitful discussions. We acknowledge funding support from the USA National Science Foundation (Award 2015557). We thank the Center for Computational Innovations at RPI for providing computational facilities.

References

[1] S.M. Wiederhorn, L.H. Bolz, Stress Corrosion and Static Fatigue of Glass, Journal of the American Ceramic Society 53 (1970) 543–548. https://doi.org/10.1111/j.1151-2916.1970.tb15962.x.

[2] C.L. Thorpe, J.J. Neeway, C.I. Pearce, R.J. Hand, A.J. Fisher, S.A. Walling, N.C. Hyatt, A.A. Kruger, M. Schweiger, D.S. Kosson, C.L. Arendt, J. Marcial, C.L. Corkhill, Forty years of durability assessment of nuclear waste glass by standard methods, Npj Mater Degrad 5 (2021) 1–28. https://doi.org/10.1038/s41529-021-00210-4.

[3] Intel, Intel Unveils Industry-Leading Glass Substrates to Meet Demand for More Powerful Compute, Newsroom (2023). https://newsroom.intel.com/artificial-intelligence/intel-unveils-industry-leading-glass-substrates (accessed March 29, 2025).

[4] S.M. Wiederhorn, H. Johnson, A.M. Diness, A.H. Heuer, Fracture of Glass in Vacuum, Journal of the American Ceramic Society 57 (1974) 336–341. https://doi.org/10.1111/j.1151-2916.1974.tb10917.x.

[5] Z. Huang, M. Tomozawa, Internal friction at crack tip of soda-lime silicate glass, Journal of Non-Crystalline Solids: X 25 (2025) 100219. https://doi.org/10.1016/j.nocx.2025.100219.

[6] T. To, F. Célarié, C. Roux-Langlois, A. Bazin, Y. Gueguen, H. Orain, M. Le Fur, V. Burgaud, T. Rouxel, Fracture toughness, fracture energy and slow crack growth of glass as investigated by the Single-Edge Precracked Beam (SEPB) and Chevron-Notched Beam (CNB) methods, Acta Materialia 146 (2018) 1–11. https://doi.org/10.1016/j.actamat.2017.11.056.

[7] R.J. Charles, Static Fatigue of Glass. I, Journal of Applied Physics 29 (1958) 1549–1553. https://doi.org/10.1063/1.1722991.

[8] R.J. Charles, Static Fatigue of Glass. II, Journal of Applied Physics 29 (1958) 1554–1560. https://doi.org/10.1063/1.1722992.

[9] W.B. Hillig, The C-H delayed failure mechanism revisited, Int J Fract 139 (2006) 197–211. https://doi.org/10.1007/s10704-006-0025-3.

[10] W.B. Hillig, Model of effect of environmental attack on flaw growth kinetics of glass, Int J Fract 143 (2007) 219–230. https://doi.org/10.1007/s10704-006-9020-y.

[11] K.-T. Wan, S. Lathabai, B.R. Lawn, Crack velocity functions and thresholds in brittle solids, Journal of the European Ceramic Society 6 (1990) 259–268. https://doi.org/10.1016/0955-2219(90)90053-I.

[12] M. R'Mili, J. Lamon, Investigation of subcritical crack growth using load relaxation tests on fiber bundles, Acta Materialia 59 (2011) 2850–2857. https://doi.org/10.1016/j.actamat.2011.01.024.

[13] A. Mesgarnejad, A. Imanian, A. Karma, Phase-field models for fatigue crack growth, Theoretical and Applied Fracture Mechanics 103 (2019) 102282. https://doi.org/10.1016/j.tafmec.2019.102282.

[14] Y.-S. Lo, M.J. Borden, K. Ravi-Chandar, C.M. Landis, A phase-field model for fatigue crack growth, Journal of the Mechanics and Physics of Solids 132 (2019) 103684. https://doi.org/10.1016/j.jmps.2019.103684.

[15] S.J. Grutzik, K.T. Strong, J.M. Rimsza, Kinetic model for prediction of subcritical crack growth, crack tip relaxation, and static fatigue threshold in silicate glass, Journal of Non-Crystalline Solids: X 16 (2022) 100134. https://doi.org/10.1016/j.nocx.2022.100134.

[16] E.C.C.M. Silva, J. Li, D. Liao, S. Subramanian, T. Zhu, S. Yip, Atomic Scale Chemo-mechanics of Silica: Nano-rod Deformation and Water Reaction, J Computer-Aided Mater Des 13 (2006) 135–159. https://doi.org/10.1007/s10820-006-9008-y.
[17] Y.-A. Zhang, J. Tao, X. Chen, B. Liu, Mixed-pattern cracking in silica during stress corrosion: A reactive molecular dynamics simulation, Computational Materials Science 82 (2014) 237–243. https://doi.org/10.1016/j.commatsci.2013.09.045.
[18] F. Molaei, J. Kemeny, Investigation of Stress Corrosion Cracking in rocks, a reactive molecular dynamic simulation: 55th U.S. Rock Mechanics / Geomechanics Symposium 2021, 55th U.S. Rock Mechanics / Geomechanics Symposium 2021 (2021). http://www.scopus.com/inward/record.url?scp=85123052100&partnerID=8YFLogxK (accessed April 1, 2025).
[19] J.M. Rimsza, R.E. Jones, L.J. Criscenti, Chemical Effects on Subcritical Fracture in Silica From Molecular Dynamics Simulations, Journal of Geophysical Research: Solid Earth 123 (2018) 9341–9354. https://doi.org/10.1029/2018JB016120.
[20] L.B. Freund, Dynamic Fracture Mechanics, Cambridge University Press, Cambridge, 1998.
[21] E. Sharon, J. Fineberg, Confirming the continuum theory of dynamic brittle fracture for fast cracks, Nature 397 (1999) 333–335. https://doi.org/10.1038/16891.
[22] LAMMPS, (2025). www.lammps.org.
[23] G. Wahnström, Molecular-dynamics study of a supercooled two-component Lennard-Jones system, Phys. Rev. A 44 (1991) 3752–3764. https://doi.org/10.1103/PhysRevA.44.3752.
[24] M. Dzugutov, S.I. Simdyankin, F.H.M. Zetterling, Decoupling of diffusion from structural relaxation and spatial heterogeneity in a supercooled simple liquid, Physical Review Letters 89 (2002) 195701.
[25] M. Dzugutov, Formation of a Dodecagonal Quasi-Crystalline Phase in a Simple Monatomic Liquid, Physical Review Letters 70 (1993) 2924–2927.
[26] M. Dzugutov, Glass-Formation in a Simple Monatomic Liquid with Icosahedral Inherent Local Order, Physical Review A 46 (1992) R2984–R2987.
[27] Y.F. Shi, M.L. Falk, Atomic-scale simulations of strain localization in three-dimensional model amorphous solids, Physical Review B 73 (2006) 214201.
[28] Y. Shi, J. Luo, F. Yuan, L. Huang, Intrinsic ductility of glassy solids, Journal of Applied Physics 115 (2014) 043528. https://doi.org/10.1063/1.4862959.
[29] Y. Shi, Creating Atomic Models of Brittle Glasses for In Silico Mechanical Tests, International Journal of Applied Glass Science 7 (2016) 464–473. https://doi.org/10.1111/ijag.12253.
[30] M. Akl, L. Huang, Y. Shi, Brittle to ductile transition during compression of glassy nanoparticles studied in molecular dynamics simulations, Journal of Applied Physics 134 (2023) 035104. https://doi.org/10.1063/5.0151127.
[31] B. Deng, Y. Shi, On measuring the fracture energy of model metallic glasses, Journal of Applied Physics 124 (2018) 035101. https://doi.org/10.1063/1.5037352.
[32] J. Luo, K. Dahmen, P.K. Liaw, Y. Shi, Low-cycle fatigue of metallic glass nanowires, Acta Materialia 87 (2015) 225–232.
[33] S. Nose, A Unified Formulation of the Constant Temperature Molecular-Dynamics Methods, J Chem Phys 81 (1984) 511–519.
[34] W.G. Hoover, Canonical Dynamics - Equilibrium Phase-Space Distributions, Physical Review A 31 (1985) 1695–1697.

[35] B. Luan, M.O. Robbins, The breakdown of continuum models for mechanical contacts, Nature 435 (2005) 929–932. https://doi.org/10.1038/nature03700.
[36] C. Feddersen, Discussion to: plane strain crack toughness testing, A.S.T.M. Spec. Tech. Publ. 410 (1967) 77.
[37] M. Isida, Analysis of stress intensity factors for the tension of a centrally cracked strip with stiffened edges, Engineering Fracture Mechanics 5 (1973) 647–665. https://doi.org/10.1016/0013-7944(73)90045-3.
[38] G.R. Irwin, Analysis of Stresses and Strains Near the End of a Crack Traversing a Plate, Journal of Applied Mechanics 24 (1957) 361–364. https://doi.org/10.1115/1.4011547.
[39] G.R. Irwin, H. Liebowitz, P.C. Paris, A mystery of fracture mechanics, Engineering Fracture Mechanics 1 (1968) 235–236. https://doi.org/10.1016/0013-7944(68)90027-1.
[40] P.C. Paris, G.C.M. Sih, Stress analysis of cracks, A.S.T.M. Spec. Tech. Publ. 381 (1965) 52.
[41] B.R. Lawn, Diffusion-controlled subcritical crack growth in the presence of a dilute gas environment, Materials Science and Engineering 13 (1974) 277–283. https://doi.org/10.1016/0025-5416(74)90199-2.
[42] B.R. Lawn, Physics of Fracture, Journal of the American Ceramic Society 66 (1983) 83–91. https://doi.org/10.1111/j.1151-2916.1983.tb09980.x.
[43] S.M. Wiederhorn, Subcritical Crack Growth in Ceramics, in: R.C. Bradt, D.P.H. Hasselman, F.F. Lange (Eds.), Fracture Mechanics of Ceramics: Volume 2 Microstructure, Materials, and Applications, Springer US, Boston, MA, 1974: pp. 613–646. https://doi.org/10.1007/978-1-4615-7014-1_12.
[44] H. Eyring, The Activated Complex in Chemical Reactions, The Journal of Chemical Physics 3 (1935) 107–115. https://doi.org/10.1063/1.1749604.
[45] D. Turnbull, M.H. Cohen, On the Free-Volume Model of the Liquid-Glass Transition, The Journal of Chemical Physics 52 (1970) 3038–3041. https://doi.org/10.1063/1.1673434.
[46] S.M. Wiederhorn, P.R. Townsend, Crack Healing in Glass, Journal of the American Ceramic Society 53 (1970) 486–489. https://doi.org/10.1111/j.1151-2916.1970.tb15996.x.